ELSEVIER

Biophysical Chemistry 125 (2007) 1 – 12

Biophysical Chemistry

http://www.elsevier.com/locate/biophyschem

Photophysics of ANS. I. Protein–ANS complexes: Intestinal fatty acid binding protein and single-*trp* mutants

Elena Klimtchuk, Sergei Venyaminov, Elizabeth Kurian ✠, William Wessels, William Kirk *, Franklyn G. Prendergast

Mayo Clinic College of Medicine, Rochester Minn. 55902, USA

Received 18 January 2006; received in revised form 26 July 2006; accepted 31 July 2006
Available online 12 August 2006

Abstract

We continue investigations into the physical chemistry of intestinal fatty acid binding protein, I-FABP, and its interaction with ANS and other ligands [*cf* references [Kirk, W., E. Kurian, and F. Prendergast. 1996. Characterization of the sources of protein-ligand affinity: 1-sulfonato-8-anilinonaphthalene binding to intestinal fatty acid binding protein. Biophys. J. 70: 69–83., Kurian, E., W. Kirk, and F. Prendergast. 1996. Affinity of fatty acid for rRat intestinal fatty acid binding protein: Further examination. Biochemistry. 35:3865–74]. The photophysics of the *wt* protein is compared with that in two mutants which lack respectively one or the other of two *trp* moieties, one of which, *trp* 82, is located near the binding region for the polar head group of ligands. These studies afford a look into how the fluorescence of the *wt* protein is established, that is, as an almost direct sum of the fluorescence of the two individual *trp* residues, and how this fluorescence is quenched upon binding to ANS. Though we have access to all the relevant spectroscopic and geometric information necessary to specify in detail the Foerster–Dexter energy transfer model, the quenching process is not explicable in terms of very-weak coupling, as is usually assumed in fluorescence studies in protein systems, but in terms of a stronger effect which goes beyond the simple very-weak dipole:dipole formalism. The quenching of *trp* emission by bound ANS is not as great as that anticipated by ordinary resonance energy transfer, neither is the quenching observed in the reduced lifetimes of the *trp* emission upon ANS binding as great as that observed in steady-state intensity. However the observed steady-state quenching is explicable in terms derived from the lifetime measurements, together with observed spectral band shifts, by the exciton coupling model we invoke here.
Published by Elsevier B.V.

Keywords: 1,8 ANS; Non-Foerster energy transfer; Exciton coupling

We have extended our studies of the interaction of intestinal fatty acid binding protein (I-FABP) and ligands, especially 1,8 ANS (1-sulfo, 8-phenylaminonaphthalene). The purpose of this paper is to investigate the specific involvement of *trp* residues in the thermodynamics of I-FABP-ligand interactions, with a long-range view to attempting to understand some of the photophysical characteristics we have already observed in the wild type (*wt*) protein with ANS [1]. To that end, we employ specific *trp*-to-*tyr* mutants of I-FABP, and compare our results to those of our previous study with *wt* I-FABP. Since the *wt* protein has *trp* situated at two positions, we substitute alternatively one or the other *trp* with *tyr* residues, and as a control, substitute both *trp* residues with *tyr*. Single-*trp* mutants should simplify the photophysics with ANS, we reason. We shall refer to the specific *trp*-to-*tyr* mutants employed herein by the common usage WxxY, where the 'xx' gives the canonical residue position in the *wt* protein sequence.

It has been hypothesized that *trp*-82, which is closely situated near a 'cuff' of aromatic residues at the polar-head-group end of the fatty acid binding cavity, may be crucial in establishing the folding pathway of the *wt* protein [2]. In addition, this same *trp* makes a hydrogen-bond to a highly-conserved, and, at least on the time-scale of molecular dynamics simulations, essentially immobile structural water molecule [3–5]. Thus, the folding and stability, as well as ligand-binding affinity of the W82Y mutant, is of some interest in its own right.

Abbreviations: NMR, nuclear magnetic resonance; CD, circular dichroism; ANS, 8-anilino1-sulfonaphthalene; I-FABP, rat intestinal fatty acid binding protein; uv, ultraviolet; FTIR, Fourier Transform infrared spectroscopy.

* Corresponding author.
E-mail address: kirk.william@mayo.edu (W. Kirk).
✠ Deceased.

0301-4622/$ - see front matter. Published by Elsevier B.V.
doi:10.1016/j.bpc.2006.07.016

ANS is a very widely used fluorescence probe, yet, despite this popularity, significant questions remain concerning its binding selectivity for hydrophobic 'patches' as well as the precise origin of its enhanced quantum yield when bound to such regions. We already observed fluorescence energy transfer from *trp* to ANS in the *wt* protein, and we now have access to structural data from a recent NMR study of the solution structure of I-FABP complexed with ANS, performed in this laboratory [6]. This latter study yields a distribution of distances and orientations of the ANS naphthalene moiety with respect to the *trp* residues of the *wt* protein, hence we have all the information we need to deduce quantitative predictions of energy transfer efficiencies, which we can then compare to direct measurements of quenching via steady-state or time-resolved (lifetime) techniques. We specifically address the following questions in this contribution: 1) Do the mutants fold like the *wt* protein, and do they bind ANS and oleic acid similarly to the *wt* protein? These are structural and functional 'control' questions, necessarily underlying any use of mutant proteins to address structure/function questions about *wt* proteins; 2) Are the *wt* fluorescence properties explicable in terms of contributions from each *trp* e.g. are the two residues additive?; 3) Is the observed quenching of *trp* by ANS explicable in terms of dipole–dipole energy transfer alone, or are other mechanisms (due, say, to the near proximity of *trp* 82 in the binding pocket) operative? We report here the CD and FTIR spectra and secondary-structure fittings for W82Y, W6Y, and the double mutant W6YW82Y, as well as thermal denaturation temperatures (providing a measure of the 'stability') for these proteins. We report on assays for the ligand-binding affinity of the mutant proteins, demonstrating their functional similarity with *wt*. We also report on fluorescence lifetime measurements on these mutant proteins, either in the *apo* form or as bound 1,8 ANS, as well as the steady-state fluorescence spectra in these systems.

In the second and later contributions (seq. II, III, IV, V.), we utilize the information presented here, supplemented by additional studies, to address more specifically the photophysics of ANS itself (and comparable compounds), namely the spectral properties in solution and as bound to I-FABP, the nature of the underlying transitions (in II,) a quantitative reconstruction of the unusually strong near uv CD as shown in this paper (in III), and an analysis of the fluorescence decay characteristics of ANS in solvents and its probable mechanisms (in IV, and, with respect to protein-bound ANS in V). In these studies we attempt to quantitatively fit, and even predict, spectral and rate parameters using recent theories of solvent-controlled dynamics in electron transfer reactions, and include a theoretical model of our own to attack the problem of Gaussian-distributed emission lifetimes.

1. Materials and methods — experimental rationale

E. coli strain MG 1655 containing the pMON-IFABP vector and the singly-mutated pMON-IFABP vectors were kindly provided by the Frieden lab. at Washington Univ. Sch. Med. (St. Louis). The double mutant W6Y-W82Y was prepared by digesting the single mutant plasmids with pPum1 and Xba1 restriction enzymes (Sigma, St. Louis.) and then ligating. An automated Sequencer analyzed the double mutant DNA to demonstrate the sequence conformity with the expected result. Wild type I-FABP as well as the three mutants were expressed and purified as described [1,4]. No impurities were found on SDS PAGE gels or via TOF MS (as performed by an in-house facility — data not shown).

Protein concentrations were obtained by quantitative nitrogen determinations [7], based upon ashing protein samples with boiling $HClO_4$, followed by direct photometric analysis of ammonia evolved by the indophenol blue method. Nitrogen content calculated from the sequence data then yielded, via comparison with the uv-absorption spectrum, the following molar absorptivities at 280 nm: *wt*: 18,700 [1]; *W6Y* 13360; *W82Y* 13520; *W6YW82Y* 10500 M^{-1} cm^{-1}. The errors are roughly ±5%. 8-Anilinonapthalene-1-sulfonate ammonium salt was from Fluka (Ronkonkoma NY), $\varepsilon_{350}=4995\pm10$ in neutral water. Stock solutions of oleic acid (Avanti Polar Lipids, Birmingham Ala) were prepared as described [8], and all other reagents were commercially supplied high purity grade. We employed 10 mM potassium phosphate buffer, pH 7, for all studies reported here.

Circular dichroism (CD) measurements in the far uv region were performed on a JASCO J-710 spectropolarimeter with an RTE-111 Neslab circulating water bath for temperature control. Measurements were conducted in a 233 μm path length quartz cell at protein concentrations ~ 50 μM over the temperature range from 5–80 °C. Four methods of secondary structure calculation were employed for the data interpretation.

We discuss below our more detailed investigations of relative binding affinity for the mutant proteins *vs* the wild type. Here we wish to describe experiments conducted in an attempt to corroborate these results with CD measurements. There being a strong signal evident in the near uv CD of wild type protein upon interaction with ANS (*vide infra*), it is possible to calculate the dissociation constant K values from these data. The technique employed is essentially similar to that used earlier [1,8,9] with fluorescence, whereby now the ellipticity of ANS at a given wavelength obtained per mole of protein is ascertained, as a function of added ANS concentration, or θ_{tota}.

$$\theta_{tota} = (\theta_{compl}-\theta_{apo})(nA + P + K - \{(nA-P+K)^2 + 4PK\}^2)/2P + \theta_{apo}. \quad (1)$$

θ_{compl} is the ellipticity that would be obtained for the 1:1 ANS/I-FABP complex at saturation, and θ_{apo} is the ellipticity of the uncomplexed protein. The ANS dissociation constant 'K' obtained here, and the stoichiometric factor 'n', which effectively absorbs variations in the ANS concentration between identical runs, is to be compared with that obtained from techniques described below. 'P' and 'A' refer to the protein and ANS concentrations.

It should be noted that this analysis is based on two single-point measurements, and hence subject to a bit more 'noise' than those discussed below, which are based on integrated fluorescence spectra.

Steady-state fluorescence spectra, as well as uv–vis. absorption spectra were performed as described (1). Briefly, the

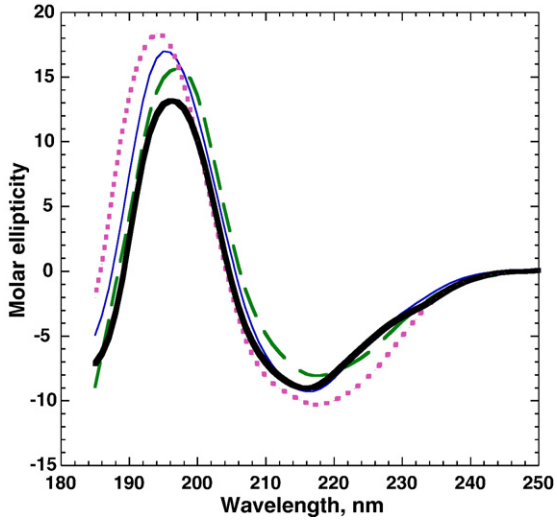

Fig. 1. Far uv CD spectra of 50 μM I-FABP) (−−−−− − *wt*, (− − − −) − W82Y, (———) − W6Y (. . . . .) − W6YW82Y. For all figures the buffer conditions are pH 7.5 10 mM Na–phosphate. Molar per residue ellipticity is given in kdeg cm^2 $dmol^{-1}$ for all Figures.

protein/ANS dissociation constants for the mutants (cf. Table 2) were calculated by fitting the data as in Fig. 1. According to the equation (*cf.* 1):

$$df = \{nP + A + K - [(nP - A + K)^2 + 4AK]^{1/2}\}/[2A/(\phi - 1)], \quad (2)$$

where *df* is the relative fluorescence of a sample at a given concentration of added protein: or: $\{\mathbf{F}([P];ANS) - \mathbf{F}([0];ANS)\}/(\mathbf{F}([0];ANS) - \mathbf{F}([0];0))$; where the **F** 's are the integrated fluorescence (e.g. 390 nm–650 nm), $\phi - 1$ is the effective fluorescence enhancement of a sample relative to a solution without added.

For the calculation of protein/Fatty Acid dissociation constant (K_{FA}), the following expressions [8] were used:

$$K_{FA} = (1/N)\Sigma\ K\ x_i\{F_i - P_i + P_i[x_i + K\ x_i/(A_i - P_i\ x_i)]\} / [(A_i - P_i\ x_i)(1 - x_i) - Kx_i] \quad (3)$$

where N is the number of additions of ANS, P_i, F_i, and A_i are the total concentrations of protein, fatty acid, and ANS, respectively, at each i-th ANS addition, K was determined as described above, and x_i is the fraction of protein bound to ANS at each addition:

$$x_i = (\mathbf{F}([P-F]_i; ANS) - \mathbf{F}([P-F]_i; 0) - A_i q]/P_i q(\phi - 1) \quad (4)$$

with $q = 0.14$ the slope of the relative fluorescence of a solution of FA at given concentration as a function of the concentration of ANS added (on our instrument in relative units i.e. in 10^6 cps/μM ANS), $\mathbf{F}([P-F]_i;ANS)$ and $\mathbf{F}([P-F]_i;0)$ — the fluorescence of protein/fatty acid complex in the presence and absence of ANS, and ϕ is the same fluorescence enhancement factor as introduced above.

To determine the efficiency of energy transfer, in the case of ANS binding to the mutant proteins, we could have recourse to direct comparison of the emission intensities of *trp* emission and ANS emission. The problem with this approach is that there is no wavelength where one may excite *trp* residues exclusively without also exciting the bound ANS, so a correction would have to be made due to the proportion of ANS fluorescence resulting from 'bleedthrough' excitation. In addition, there have to be corrections for the quantum yield (QY) of *trp* when ANS is bound (beyond that due to the energy-transfer process), and the QY of bound ANS. We have measured this last quantity in wild-type protein, but it would require separate measurements with the mutant proteins (which do not as readily saturate as *wt*), to employ this direct method. An alternative method would be to measure only the *trp* fluorescence in the presence of various concentrations of ANS. This assumes that all the quenching observed is due to energy transfer, and hence that there is no correction to the *trp* QY when ANS is bound. Since we already have ascertained the value for the dissociation constant for ANS, or K, we can utilize a linearly transformed binding equation which allows facile determination of the one remaining unknown, the energy-transfer efficiency, or η, rather than employ the less robust nonlinear least-squares analysis from the full quadratic formula (which involves two variables). If we let the ratio of fluorescence in the presence to absence of a given amount of ANS be written $\mathbf{F}(A_i)/F(0)$ and define $1 - \mathbf{F}(A_i)/F(0) = f(A_i)$; then:

$$f(A_i) = \eta - (K/P)\eta f(A_i)/[\eta A_i/P - f(A_i)] \quad (5)$$

It will be noticed that the analysis resembles that behind a Scatchard plot — the intercept on the abscissa ($f(A)$ axis) is the value of η. In practice, a value is chosen for η in the denominator, and the fitted value is inserted in a next iteration, and the iteration process continued until the two values are consistent. In fact, the first iteration is often sufficiently robust.

Time-resolved fluorescence decays for the proteins were measured using single-photon counting [10] with sample excitation at 295 nm using the frequency-doubled output of a Coherent model 700 rhodamine dye laser pumped by the frequency-doubled output of a Coherent Antares YAG laser (Coherent, Palo Alto, CA). The fluorescence emission at 350 nm, or at 520 nm for ANS, was observed through a 10-nm bandpass optical filter. The protein concentration for time-resolved measurements was 10 μM. Data analysis was provided by using the Globals Unlimited program [11] with the fluorescence intensity decay represented as a sum of exponentials. Later, we shall have recourse to a distributed decay model (a Gaussian), but for our purposes, a sum of exponentials should suffice, since we are here only interested in comparing net decay rates of the mutant proteins with and without ANS bound.

A Bio-RAD FTS-40 FTIR spectrometer was used for infrared spectroscopy. This basic system was customized with a shuttle system as previously described.

We employed 3.6 μm CaF_2 cells and a water-absorbance correction as described [12]. All samples were at 25 °C, and the protein concentration employed was 1 mM. Secondary structure was calculated using the method of Kalnin et al. [13] implemented via two different mathematical approaches.

2. Results and discussion

2.1. Secondary structure and stability of IFABP trp mutants

The replacement of tryptophan by tyrosine in IFABP reduces the protein stability in the presence of urea (by 1.2 kJ/mol for W82Y, and by 4 kJ/mol for W6Y) [2]. Our studies on thermostability of the mutants by measuring the temperature dependence of CD signal at 222 nm (data not shown) demonstrate that heat denaturation was accompanied by irreversible aggregation at temperatures above 70 °C for *wt.* IFABP, above 65 °C for the two single mutants, and above 60 °C for the double mutant (W6Y/W82Y). Due to the appearance of these two processes the slight difference in temperatures (*ca* 3–5 °C) between the *wt* and mutants' melting curves could be assigned to the slight difference in their stability as well as their ability to aggregate.

We employed far uv CD, and FTIR measurements to check if W6Y, W82Y and W6Y/W82Y fold like the *wt* protein. Fig. 1 shows some differences in the far uv CD between the mutants and *wt.* However, these differences do not translate into substantially different secondary structure predictions, as shown in Table 1. There we give the results of protein secondary structure calculations using four different mathematical methods for fitting the CD data, and two methods for fitting the IR spectra. Our results are compared with those based on X-ray data for wild type I-FABP [13] The methods employ different mathematical models and each of them operate with an independent, and not completely overlapping, basis set of reference proteins, which makes it problematic to evaluate the relative accuracy of each method, except on a case by case basis.

As one can see, though the different methods give rather divergent results for each protein, within the results for each method (labelled as A, B, etc.) there are very similar structural assignments for the mutants and *wt*. The observed differences in the CD spectra (Fig. 1) might thus be due to minor changes in secondary structure upon mutation — however, it is quite possible that they are due to the differential contribution of tyrosine *vs* tryptophan to the far uv signal. Thus though they make some difference in the total ellipticity, they are not resolved by any of the secondary structure algorithms to actual components of secondary structure, which are essentially the same predicted values in any one algorithm. This effect of 'aromatic far uv signal' might be the source of the observed overestimation of α-helix content at the expense of estimated β-sheet, when compared with the Kabsch–Sander X-ray assignment of secondary structure percentages in the *wt* I-FABP [14,15]. In that regard, secondary structure deduced from IR data coincide better with the Kabsch–Sander [15] structure-content evaluation for *wt*, probably due to the fact that the IR spectra are corrected for absorbance of side chain substituents, and tryptophan for all practical purposes does not contribute to the amide I and amide II IR absorbance bands.

To summarize, for the mutant proteins, the same high proportion of β-sheet together with a small amount of α-helix in the mutants is observed, as per the wild-type protein, and this proportion closely resembles that seen in the *wt* structure from the crystallography.

Our studies of heat denaturation and the calculation of protein secondary structure suggest that these point mutations do not radically alter the protein's ability to fold into a structure similar to *wt* I-FABP. Moreover, addition of any amount of ANS to the protein solutions did not produce noticeable difference in far uv CD spectra (data not shown) nor in the heat denaturation processes (data not shown) whether in *wt* or in mutant proteins, probably because the proteins thermally

Table 1
Secondary structure of I-FABP and predicted values for mutants

Protein	% Secondary structure category present											
	α-helix			β-sheet			β-turn			Random coil		
	Method/analysis package*:											
	X-ray	CD	IR	X-ray	CD	IR	X-ray	CD	IR	X-ray	CD	IR
wt	11	29^{A}†	0^{E}	58	42^{A}	54^{E}	15	18^{A}	0^{E}	15	18^{A}	44^{E}
		26^{B}	11^{F}		67^{B}	51^{F}		4^{B}	5^{F}		4^{B}	33^{F}
		28^{C}			34^{C}			16^{C}			21^{C}	
		15^{D}			41^{D}			21^{D}			24^{D}	
W6Y		27^{A}	0^{E}		61^{A}	58^{E}		8^{A}	8^{E}		8^{A}	33^{E}
		16^{B}	1^{F}		80^{B}	54^{F}		4^{B}	10^{F}		4^{B}	34^{F}
		26^{C}			36^{C}			21^{C}			19^{C}	
		18^{D}			38^{D}			26^{D}			22^{D}	
W82Y		31^{A}	12^{E}		46^{A}	64^{E}		19^{A}	14^{E}		19^{A}	10^{E}
		21^{B}	13^{F}		61^{B}	56^{F}		9^{B}	15^{F}		9^{B}	16^{F}
		24^{C}			32^{C}			21^{C}			19^{C}	
		17^{D}			36^{D}			24^{D}			24^{D}	
W6YW82Y		31^{A}	ND		50^{A}	ND		8^{A}	ND		8^{A}	ND
		26^{B}	ND		62^{B}	ND		10^{B}	ND		10^{B}	ND
		30^{C}			30^{C}			18^{C}			18^{C}	
		25^{D}			26^{D}			24^{D}			28^{D}	

*The X-ray defined secondary structure was provided by the Kabsch and Sander (13) algorithm applied to *wt*. I-FABP. *A* represents application of the package CONTIN [23]; *B* is the application of VARSLC routine from Manavalan and Johnson [24]; *C* is the SELCON3 program from Steerama et al. [25];*D* is the SVD algorithm implemented from Hannessey and Johnson [26]; In the i.r. measurements *E* is the SVD method and *F* the CONTIN algorithm as implemented in Kalnin et al. [13]. For a review, see Venyaminov and Yang [27], see also [28].

denature only at relatively high temperatures in any case. This finding suggests that no significant changes occur in I-FABP's secondary structure upon ANS binding.

2.2. Near uv CD spectra, analysis and ligand binding

Addition of ANS to all four proteins dramatically changes the CD spectrum in the near uv-to-visible range. As an example, CD titration spectra of *wt* I-FABP upon serial additions of ANS are presented in Fig. 2A; A very large negative peak appears in the absorption region of Trp and ANS at ~ 280 nm. One positive and one negative CD band appear to the red of this region at ~ 340 and ~ 380 nm, respectively, which corresponds only to ANS absorption. Similarly large Cotton effects were demonstrated in this region by all three mutant–ANS complexes (Fig. 2B). However, the negative band around 380 nm was observed only for the complexes of ANS with *wt* or W6Y. The W82Y and W6YW82Y proteins, whose *trp*-82 inside the binding pocket is substituted by tyrosine, show only positive CD bands in the (~ 340 nm) range upon ANS binding (Fig. 2B). While it is in later contributions (II, III) where we discuss the physical ramifications of these results in more detail, there are two important results to which we wish to draw attention here. The first is that the alternating sign of the Cotton effect in the naphthalenic absorption allows us to assign which part of the absorption spectrum of bound ANS represents naphthalene L_b and L_a, (which are generally taken to be orthogonal), a point which will become important with respect to energy-transfer probability calculations below. Secondly, the mere appearance of a significant CD in this region, tied so closely to the presence of *trp* in the pocket suggests some type of electronic coupling which may be stronger than the very-weak dipole:dipole

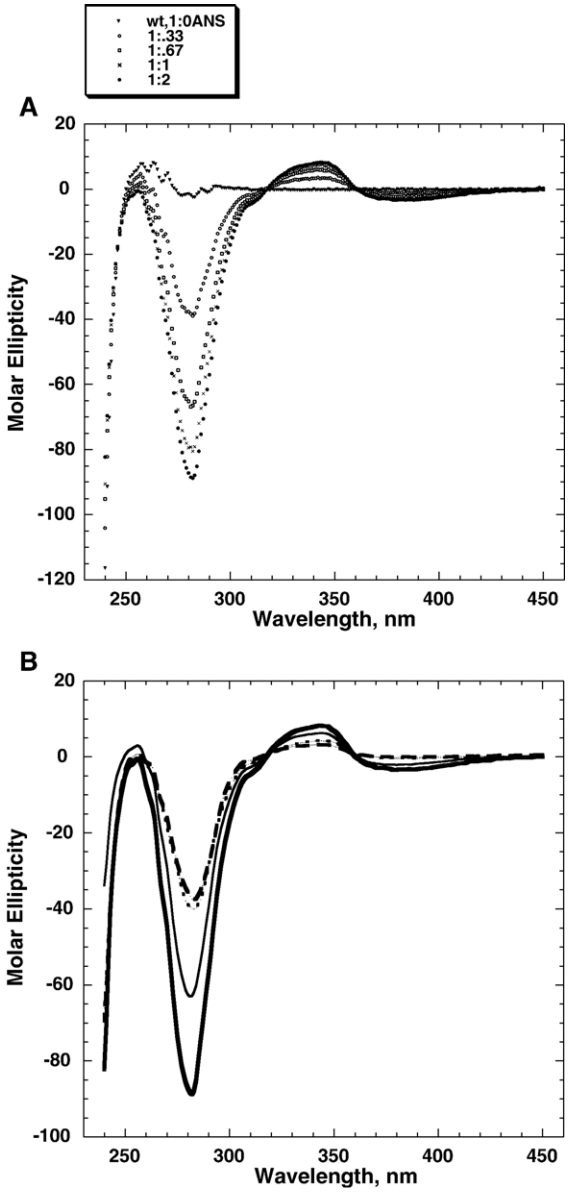

Fig. 2. A) CD 'titration' of 44 μM *wt* I-FABP with ANS, at mole ratios of 1:1/3, 1:2/3, 1:1, 1:3/2, and 1:2, respectively. Fig. 2B) Molar ellipticity spectra per mol protein at ~ 50 μM Protein, 100 μM ANS, for *wt*. (———), W6Y (———), W82Y (- - - - -), and W6YW82Y (.....).

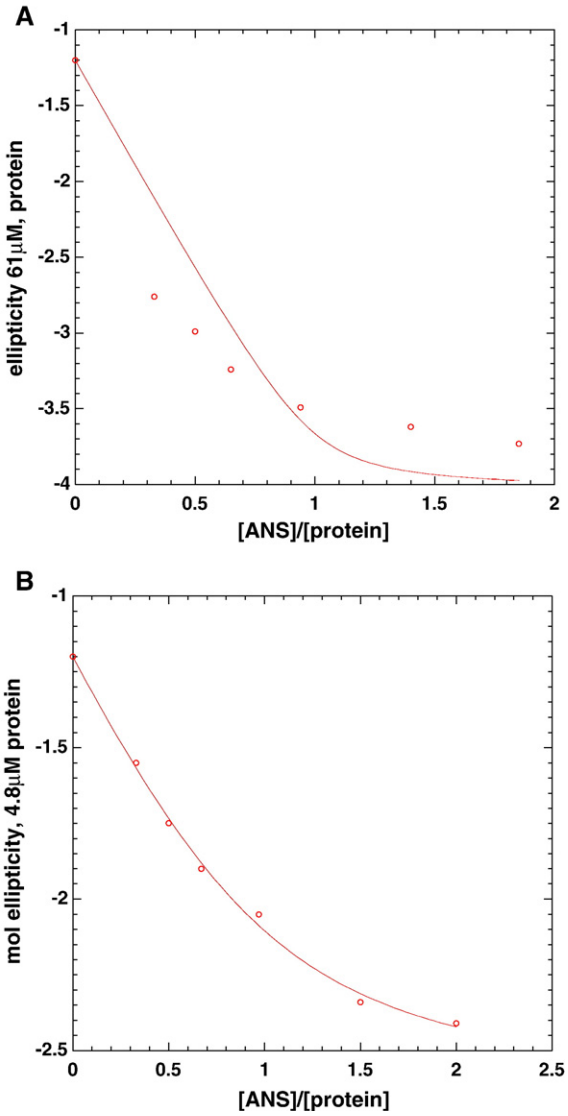

Fig. 3. Molar ellipticities (per mol. protein) at 280 nm *vs* [ANS]/[protein] of W82Y at A) 61 μM, and B) 4.8 μM. Circles are experimental data and thin lines are fits to data from Eq. (1) text, for 1:1 stoichiometry.

coupling approximation used in the Foerster–Dexter mechanisms usually employed.

We have also put this significant CD signal to more practical uses. The titration of CD signal with added protein or ANS can simply be used to determine dissociation constants for the mutant proteins, and these values compared with those obtained by our other methods [1,8].

The results of CD titrations of I-FABP by ANS at protein concentrations of 61 μM, and 4.8 μM are shown on Fig. 3. The molar ellipticity at 280 nm is plotted *vs* [ANS]/[Protein] ratios for W82Y.

Fitting these signals for K and θ_{compl} as per Eq. (1) employing 61 μM protein at first gave results at variance with our steady-state fluorescence results, namely significantly larger values of K were obtained, and the fits were substantially poorer, as is seen in Fig. 3A, compared with Fig. 5 from fluorescence titrations. This was puzzling, until it was realized that the amphipathic nature of ANS might lead to unspecific binding at the high concentrations of protein and ANS employed in these CD measurements (cf. [16,17]). Consequently two additional types of experiment were run: 1) A set of experiments were conducted under conditions more closely resembling those employed for fluorescence titrations (*infra*): namely, the protein concentration was decreased ten-fold to ~ 5 μM (Figs. 3B and 2) another set were performed in which different amounts of NaCl were added to the buffer and the titration was repeated. We reasoned that increasing the ionic strength might more efficiently shield charges on the protein surface, thus suppressing nonspecific binding. Such turned out to be the case (supplemental data). This also had the salutory effect of allowing our nonlinear least-square analysis of the binding Eq. (1) to proceed to a good fit (e.g. a comparably low χ^2 statistic, unlike the attempted fittings of the previous, "high concentration", data) to values much closer to those obtained by fluorescence. Table 2 presents these (more compatible) values, together with those we obtained via fluorescence.

This part of our study seems to confirm certain results of Matulis (*cf.* [16,17]): it serves as a caution for investigators who add higher and higher concentrations of ANS to proteins, that because of possible 'detergent'-like properties of ANS, unwanted side-reactions of ANS with proteins are possible, and that perhaps the kinds of titrations reported here are best accomplished by adding protein to relatively small fixed concentrations of ANS.

2.3. Fluorescence spectra, analysis and ligand binding

Fig. 4 displays a representative part of the results obtained in one titration of ANS fluorescence with W6Y protein, and Fig. 5 shows a "fit" obtained via Eq. (2) with such data. (See Materials and methods). In all the cases the stoichiometry of protein/ANS complex was 1:1. Calculated values of K for this binding process are given in Table 2.

Table 2
Ligand binding affinities

	K (ANS), μM (fluor)	K (ANS), μM (CD)	K (OA), μM
wt	3.5±1	4.5	0.014±.006
W6Y	9.3±0.9	12.5	0.49±0.1
W82Y	28.4±2.4	20.5	1.2±0.1
W6YW82Y	5.5±0.4	9.3	5.5±1.2

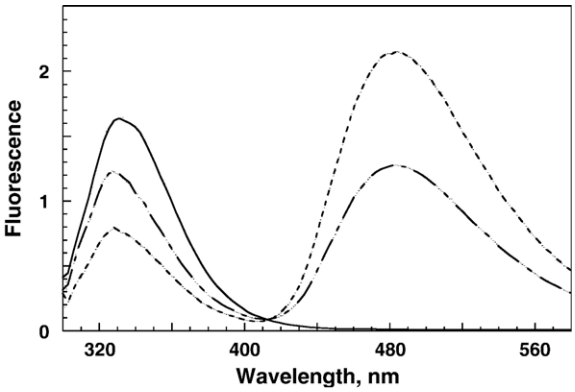

Fig. 4. Fluorescence spectra of 8.1 μM W6Y: (———), W6Y + ANS (1:6): (- - - -), and W6Y + ANS + oleic acid (–.–.–) at 1:6:1.

As one might expect, the substitution of *trp*82 — whose indole ring is located inside the binding pocket — by *tyr*, changes somewhat the local ANS environment, and, as a consequence, there is a significant drop in the ANS affinity to W82Y compared with wild type and W6Y, in which the side chain moiety of the substituted *trp* is external to the protein core. Surprisingly, the double mutant W82YW6Y shows higher affinity to ANS than either of the single mutants.

Preservation of function in the mutants was further supported by their ability to bind fatty acids. We utilized the competitive binding assay previously developed in Ref. [8]. Fluorescence titration of protein by ANS was performed in the presence of oleic acid (1:1 protein/FA ratio). The 1:1 stoichiometry for both ANS and fatty acid binding to the mutants was assumed based on a number of fluorescence and calorimetric titration studies (data not shown).

It will be seen that, although the W6YW82Y double mutant 'reverts' to near *wt* affinity for ANS, nonetheless there is continued loss of affinity for fatty acid with respect to *wt*. This suggests as we will see again, the hypothesis that the two types of binding event, i.e. binding to ANS and to fatty acids, while indeed mutually competitive, are still distinct modes.

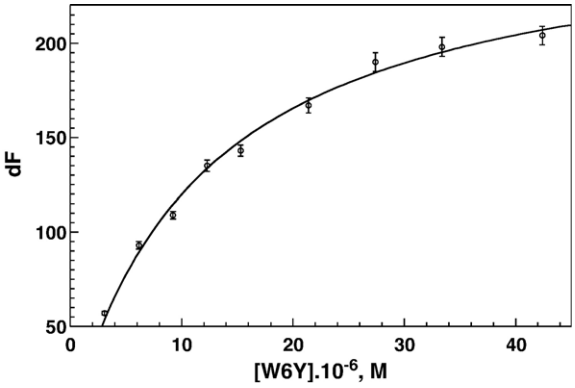

Fig. 5. Fluorescence titration of 1.4 μM ANS with W6Y protein: conditions as described in text and in Fig. 1.

2.4. Summary of various NMR results

Though we do not report the details of NMR investigations performed in this laboratory here, which have been presented elsewhere [6], the results of those studies are of great importance to the remainder of this study. It will suffice here to mention the most relevant facts for ANS binding. Wild type I-FABP was harvested from *E. coli* grown in per-deutero, ^{13}C, ^{15}N medium. Various pulse-regimes were employed to be able to fit the *apo* I-FABP solution structure. ANS was also synthesized as all ^{13}C, and perdeutero*anilino*. For *trp*-82, two major conformers were recovered, with roughly 65% and 35% probability weights. For *trp*-6 a distribution of conformations was obtained. The solution-set for these two residues relative to ANS are shown in the Fig. 6. They are plotted as functions of a fixed ANS residue. Two further results from NMR investigations are worth mentioning, inasmuch as we had already [1] intimated these possibilities. First, the sulfonate of ANS does not seem to coordinate with arg-106, as do carboxylates of bound fatty acids, but rather seems to interact with arg-126 instead, possibly through an intervening water molecule, as well as accepting a hydrogen bond from Y117 [6]; *cf* also [18]. Thus, ANS is not situated within FABP's fatty acid binding cavity in precise analogy with fatty acids. Whether the ANS binding geometry as observed in the solution structure is more representative of an 'early complex' with fatty acid (since arg-126 is from any point of view a more 'exposed' residue than arg-106), and the crystal structure is more representative of a 'late complex' with fatty acid, and whether this possibility might account for some of the time-dependence observed in stopped-flow experiments [18] while an attractive hypothesis, is still an open question. In our own competition experiments with fatty acid [8], each addition of ANS was allowed to 'incubate' for 45 min. with the protein-fatty acid 1:1 mixture, because a slow ~ 10 min equilibration was observed. As we mentioned above, the W6YW82Y mutant shows even smaller affinity for OA than the other mutants — perhaps because of 'looseness' of the cavity, *cf* [5,18], there may be no possibility to form a tighter, 'late' complex, so that the two ligands ANS and OA have essentially the same affinity.

Fig. 6. Ensemble of 'solution-set' structures from NMR data for W82 and W6 only, other parts of structure are fixed in their canonical, or X-ray coordinates. ANS is also fixed relative to the center-of mass of the protein backbone atoms in its most probable location, as determined by the NMR data.

2.5. Fluorescence lifetime and energy transfer analyses

Having ascertained that the mutant proteins are functionally similar to *wt* and maintain at least secondary structure in common with it as well, we surmised that possible excited state interactions, including dipole–dipole coupling from *trp*-to ANS could be essentially dissected by comparing the two single-*trp* mutants' photophysics in the presence and absence of saturating amounts of ANS. In Table 3 we summarized measured and calculated characteristics of IFABP mutants.

Each *trp* fluorescence decay is a sum of exponentials. While W6Y is dominated by a longer component, W82Y is dominated by a shorter one, and wild type decay is a roughly equal mixture of both of them. The steady-state *trp* fluorescence in the wild type protein is also nearly the sum of the two *trp* contributions (Fig. 7).

Fig. 8A shows the convention we followed in assigning unit (direction) vectors to transitions in ANS [19]. The contribution assigned to each of these transitions to the near uv absorption spectrum of ANS is shown in Fig. 8B (note the influence of Fig. 2 on our assignment). For *trp* transition vectors, we assigned a unit vector, located at the midpoint of the C8–C9 axis, in the direction specified by the pyrrole N-to-C-4 difference vector, which lies 46° from the above-named axis, in the indole plane [20]. We then directly calculated the value of

$$\kappa^2 = \{\mathbf{u}_{trp}{}^{\circ}\mathbf{u}_{ans} - 3(\mathbf{u}_{trp}{}^{\circ}\mathbf{R})(\mathbf{u}_{ans}{}^{\circ}\mathbf{R})/R^2\}^2, \tag{6}$$

where $\mathbf{u}$'s represent unit vectors of the indole ^1L_a or the ANS L_a/L_b transitions, and $\mathbf{R}$ is the separation vector between the ANS and indole centers. We calculated this quantity for a representative sample of *trp* residues as well as values of $|\mathbf{R}| = R$. We then assumed for *trp*-6 static distributions of R and κ^2 (which we assumed to be independent), and found the resulting static averages for either of the orthogonal transitions of ANS:

$$<\kappa^2> = (1/N_\kappa)\int \kappa^2 \exp(-(\kappa^2-\kappa_0^2)^2/2\sigma^2{}_{\kappa^2}) \tag{7a}$$

or

$$\begin{aligned}<\kappa^2> =& (1/N_\kappa)[\exp(-(\kappa_0^2)^2/2\sigma^2{}_{\kappa^2})(\kappa_0^2)\sigma_{\kappa^2} - \exp(-(4-\kappa_0^2)^2 \\ & /2\sigma^2(\kappa_0^2)\sigma_{\kappa^2} + (\sigma^2{}_{\kappa^2} + (\kappa_0^2)^2)\sqrt{2\pi}\{\mathrm{erf}[(4-(\kappa_0^2)) \\ & /\sigma_{\kappa^2}] + \mathrm{erf}[(\kappa_0^2))/\sigma_{\kappa^2}]\}] \text{ and } N_\kappa \textit{ is } \sqrt{2\pi} \\ & \times\{\mathrm{erf}[(4-(\kappa_0^2))/\sigma_{\kappa^2}] + \mathrm{erf}[(\kappa_0^2))/\sigma_{\kappa^2}]\}\sigma_{\kappa^2}\end{aligned} \tag{7b, c}$$

whilst:

$$<1/R^6> = (1/N)\int (1/R^4)\exp(-(R-R_0)^2/2\sigma_R^2)\mathrm{d}R \tag{8a}$$

The normalization factor N in Eq. (8a) is provided by the condition:

$$(1/N)\int R^2\,\wp(R)\mathrm{d}R = 1.00, \tag{8b}$$

where $\wp(R)$ is the Gaussian given in Eq. (8a). Thus, N is

$$\{R_0\sigma_R^2\exp(-R_0^2/2\sigma_R^2) + \sqrt{2\pi}R_0^2\sigma_R(1/2 + \mathrm{erf}[R_0/\sigma_R])\} \approx \sqrt{2\pi}R_0^2\sigma_R \tag{8c}$$

note that R_0 is here the center of the measured distribution of 'R' values. The NMR solution structure of IFABP gives two major conformers for *trp*-82 at 65% and 35% occupancy, with a distinct average R for each (Ref. [6] — *cf.* Fig. 3). For each indole we calculated separate values of overlap integral $J = 8.785\times10^{-25}\int\varepsilon(\lambda)f(\lambda)\lambda^4\mathrm{d}\lambda$ to each of the transitions of ANS (where '$f(\lambda)$' is the normalized fluorescence spectrum *cf* 21). Results of the calculations of the dipole–dipole interaction rate constant:

$$k_{\mathrm{dd}} = J\langle 1/R^6\rangle[\langle\kappa^2\rangle/n]^4(Q.Y.)/\langle\tau\rangle$$

for each ANS transition are given in Table 3:

From the fluorescence quenching data (Table 3) and from the binding data (Table 2) we might expect that fluorescence of *trp*-82 in the W6Y mutant when fully bound to ANS would be essentially totally quenched (>99%), and that of *trp*-6 in W82Y would be 95% quenched. In fact we observed approximately 70± 2% quenching efficiency in W6Y (Fig. 9 shows the Scatchard plot

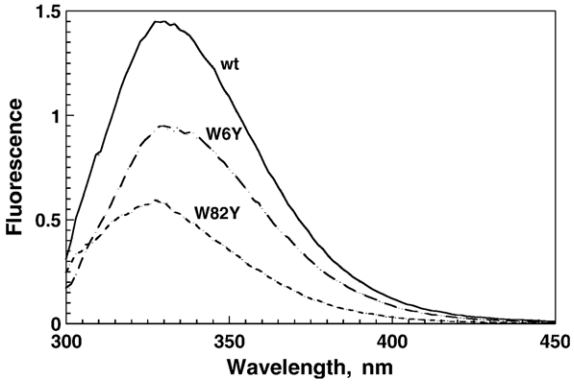

Fig. 7. W82 emission spectrum, W6Y emission, and *wt* emission at comparable protein concentrations, 295 nm excitation.

of *trp* fluorescence quenching by ANS for W6Y), and 45% in W82Y. From Table 3 we can obtain, after correction for the total amount of *trp* in the presence of bound ANS, the average lifetime $\langle\tau\rangle_{\mathrm{bd}}$ divided by the 'free' *trp* average lifetime $\langle\tau\rangle$, which yields the dynamical quenching efficiency. These are 48% for W6Y and 36% for W82Y, respectively. The failure to observe as great a quenching efficiency as one would expect for both tryptophans must be attributed to somewhat different interactions than is typically assumed for the dipole–dipole resonance energy transfer formalism.

An alternative mechanism of interaction is the coupled exciton. Call the original states $|a'b\rangle$ and $|ab'\rangle$, representing the direct product of excited *trp* and ground-state ANS in the first case, and

Table 3
Fluorescence decay data for *trp* and ANS emission

trp lifetimes

Protein	τ_1	α_1	τ_2	α_2	τ_3	$\langle\tau\rangle$	QY	$\langle\kappa^2\rangle_{1_{L_a}}$	σ_{κ^2}	$\langle\kappa^2\rangle_{1_{L_b}}$	σ_{κ^2}	$\langle R\rangle$	σ_R	$k_{\mathrm{dd}}^{(La)}$	$k_{\mathrm{dd}}^{(Lb)}$
W82Y	2.6	0.78	1.3	0.15	0.08	2.25	0.13	0.02	0.015	1.04	0.16	13.6	0.7	6.9E^7	8.4E^9
+ ANS	2.5	0.6	0.5	0.19	0.03	1.62(1.45)*									
								$^{\alpha}\kappa^2_{1_{L_a}}$	$^{\beta}\kappa^2_{1_{L_a}}$	$^{\alpha}\kappa^2_{1_{L_b}}$	$^{\beta}\kappa^2_{1_{L_b}}$	$^{\alpha}R$	$^{\beta}R$		
W6Y	5.8	0.62	2.7	0.33	0.5	4.5	0.26	1.97±.19	1.30±.03	0.05±.04	0.29±.03	5.4±.5	5.9±.1	4.16E^{12}	1.77E^{13}
+ ANS	5.2	0.46	1.8	0.12	0.08	2.66(2.3)*									
wt	5.4	0.49	1.8	0.51	–	3.56	0.19(calc.)								
+ ANS	3.8	0.73	0.92	.27		3.0									

ANS lifetimes

	τ_1	α_1	τ_2	α_2	τ_3	$\langle\tau\rangle_{\mathrm{bd}}$
W82YW6Y	19.9	0.73	7.5	0.06	0.27(fixed)	18.9
W82Y	19.4	0.67	2.9	0.02	" "	18.9
W6Y	18.2	0.38	7.0	0.03	0.27(fixed)	17.4
W6Y (300 exc.)	18.6	0.404	0.77	0.292	" "	11.1
wt	20.6	0.83	9.3	0.17		18.7

The lifetimes τ of single exponential components are shown, together with their decay amplitudes. α_3 is $1-(\alpha_1+\alpha_2)$. For all *trp* lifetimes, excitation was at 300 nm and emission monitored at 340 nm. For ANS lifetimes emission was monitored at 520 nm with excitation at 345 nm, except where noted for W6Y where a comparison is made with excitation at 300 (through *trp*). QY is the quantum yield. The χ^2 statistic for all fits presented was ≤ 1.15, for three-component fits the improvement in χ^2 obtained by using a four-component fit was less than 0.01, and for two-component fits the improvement using three-component fits was less than 0.015. For W6 (in W82Y) a distribution of distances and κ^2 is obtained, with widths (in Å for 'R') given by the respective values of σ. For W82 (in W6Y), there are two distributions about discrete conformers, labelled α and β, respectively, which have probabilities, or occupancies, of roughly 65% and 35%, respectively. The deviations given are the respective 'widths' of these distributions. Calculated values for the dipole:dipole energy-transfer rate are given in s^{-1}. 'En' is a notation for: '×10^n'. For ANS lifetimes, the protein concentration is roughly 10 μM while the ANS is 5 μM. The protein lifetimes with ANS are at 10 μM protein and 60 μM ANS. * — values in parentheses are calculated to correct for the amount of protein with ANS bound, i.e. in the case of W82Y, 79% of the protein has ANS bound to it, and for W6Y 85% does, under the experimental conditions.

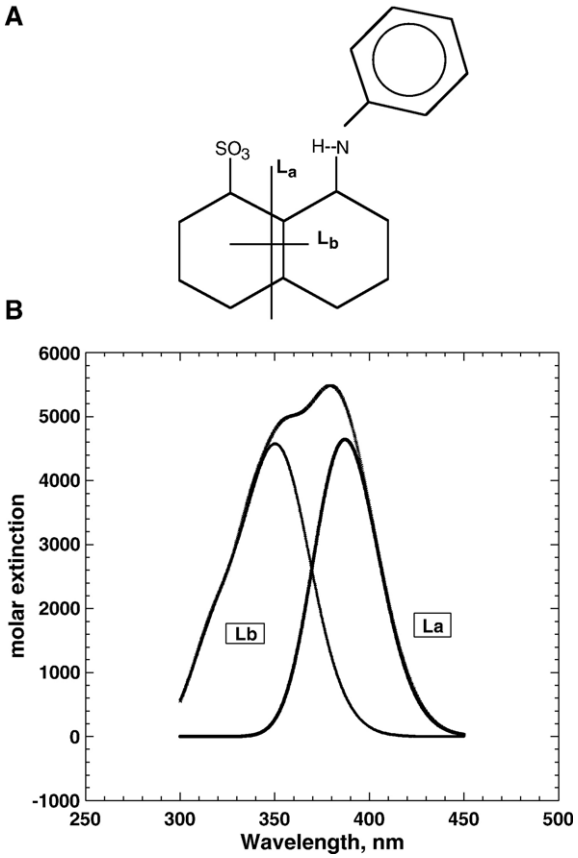

Fig. 8. A) Naphthalene transition axis convention. B) Decomposition of ANS absorption (as bound to *wt* FABP) band.

ground-state *trp* with excited-state ANS in the second case. Direct exciton interaction means that the two original (or 'old') states are coupled, i.e.$\langle a'b,_{\text{old}}|H|ab',_{\text{old}}\rangle \neq 0$, where '$H$' is the Hamiltonian for the system. However, we can rotate the two systems into a new set of states which are mutually orthogonal and stationary, that is:$\langle a'b,_{\text{new}}|ab',_{\text{new}}\rangle = 0$, and$\langle a'b,_{\text{new}}|H|ab',_{\text{new}}\rangle = 0$.

Employing Foerster's [21] treatment of the case of exciton interaction with no spatial overlap, we define a unitary transform (rotation) out of our old basis into the new, noninteracting basis:

$$\begin{matrix} |a'b\rangle,_{\text{new}} \\ |ab'\rangle,_{\text{new}} \end{matrix} = \begin{matrix} |\cos\theta & \sin\theta & | \\ |-\sin\theta & \cos\theta & | \end{matrix} \begin{matrix} |a'b\rangle,_{\text{old}} \\ |ab'\rangle,_{\text{old}} \end{matrix} \tag{9}$$

where $\tan(2\theta) = 2\langle H_{a'b,ab'}\rangle / [E_{a'b} - E_{ab'}]$ The equation for the excited state yields —

$$\begin{aligned} \Psi^{+}(t) &= c_{+}(|\, a'b\rangle,_{\text{new}})e^{-iW_{+}t/\hbar} \\ \Psi^{-}(t) &= c_{-}(|\, ab'\rangle,_{\text{new}})e^{-iW_{-}t/\hbar} \end{aligned} ; \tag{10}$$

where $W_{\pm} = (E_{a'b} + E_{ab'})/2 \pm \omega\hbar$; $\omega = -\langle H_{a'b,ab'}\rangle \csc(2\theta)/\hbar$ with the E's being the energies of the excitons of *trp* and ANS respectively, and$\langle H_{a'b,ab'}\rangle$the nonvanishing interaction energy between them, while the c's are coefficients whose squares sum to 1.00. These represent the probability at the time the two states become decoupled of the system 'landing' in either state. We have $\rho_{a'b,\text{new}} = \langle \Psi^{+}|\, \Psi^{+}\rangle$and similarly for $\rho_{ab',\text{new}}$ as the probabilities of these new states. We may now instead rewrite the $\rho,_{\text{new}}(t)$ in terms of the original states because they decay independently after vibrational relaxation (*infra*). To complete the analysis, we add a term for the decay of the old $|a'b\rangle$ exciton or the $|ab'\rangle$ exciton, i.e.

$$\rho_{a'b}(t) = [c_{+}^{2}\cos 2\theta + \sin^{2}\theta]e^{-\gamma_{a}t}, \tag{11a}$$

where γ_{a} is the decay rate of the original $|a'b\rangle$state, and the term

$$\rho_{ab'}(t) = [\cos^{2}\theta - c_{+}^{2}\cos 2\theta]e^{-\gamma_{b}t} \tag{11b}$$

for the $|ab'\rangle$ state with decay rate γ_{b}. Then the steady-state energy-transfer intensityshould be given by:

$$\int \rho_{ab'}(t)\mathrm{d}t / [\int \rho_{ab'}(t)\mathrm{d}t + \int \rho_{a'b}(t)\mathrm{d}t] \equiv \langle \rho_{ab'}(t)\rangle \tag{12a}$$

if we assume that the experiment is conducted in such a way that a' is initially excited (i.e. not counting those $|b'\rangle$states obtained by direct excitation, but only those derived from the $|a'\rangle$state by energy-transfer channels). The decay rate for protein-bound ANS is obtained from an experiment in which the ANS is 'saturated' with protein at a concentration 6× the ANS. We also make corrections based on the values previously obtained for K, for the actual concentration of bound species. One finds e.g. in Table 3 for W82Y 67% decay into 19.4 ns channel 31% into a 0.27 ns channel (fixed to be equal to that of free ANS). If the 'free' ANS is removed, then the effective lifetime of bound ANS is 18.9 ns. The fraction of ANS with 'free ANS' lifetime is larger than the actual amount of 'free' ANS as calculated from the K. Since the emission is monitored at 520 nm, however, the data is a

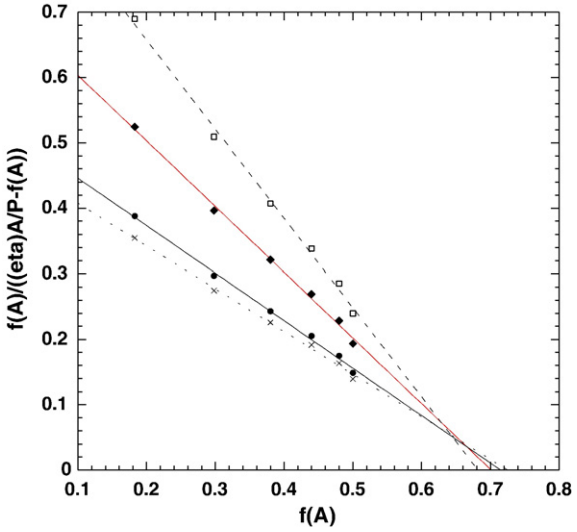

Fig. 9. Scatchard plot of quenching of integrated W6Y fluorescence by added ANS, $f(A) = 1 - \mathbf{F}(A)/\mathbf{F}(0)$. Plots obtained with several assumed values of the transfer efficiency are displayed (η in denominator of expression on ordinate is also the intercept on the abscissa). Assumed values for η are 0.8, 0.7, 0.6, and 0.5.

bit biased towards free ANS emission. A straightforward calculation from Eq. (12a) then gives:

$$<\rho_{ab'(t)}> = [\cos^2\theta - c_+^2\cos 2\theta]/[(\gamma_a/\gamma_b)(\sin^2\theta + c_+^2\cos 2\theta) + \cos^2\theta - c_+^2\cos 2\theta] \quad (12b)$$

for the $a \rightarrow b$ energy-transfer efficiency. One can see readily, that, for example, $\theta = 90°$ means that energy transfer efficiency would be roughly $1/[1+(\gamma_a/\gamma_b)]$, which would be $\sim$ 3/4 and that it is maximal at that angle, very different from the 95% or >99% quenching one would expect from the ordinary dipole: dipole energy transfer process.

Interaction of the ANS and *trp* is seen from Eqs. (9) and (10) to lead to a shift in the energy of the states as well. This may be observable in the bound absorption spectra of ANS and *trp*-82, if the red-shift of bound ANS (cf. absorption spectrum in Ref. [9]) is from this interaction, then ω, which equals $\sec 2\theta$ $[E_{a'b} - E_{ab'}]$, is roughly 890 cm^{-1} (the value of $<H_{a'b,ab'}>$ we would calculate from the $\kappa\mu_{trp}\mu_{ANS}/R^3$ interaction alone, as in our above treatment, is roughly 280 cm^{-1} for *trp*-82). The energy difference $E_{a'b} - E_{ab'}$ is determined from the spectra, such that the center of mass of the exciton density-of-states in emission is given by:

$$<\nu>_{em} = \int f(\nu)/\nu^2 d\nu / \int f(\nu)/\nu^3 d\nu \quad \text{(trp emission)} \quad (13a)$$

and in absorption by:

$$<\nu>_{exc} = \int \varepsilon(\nu) d\nu / \int \varepsilon(\nu)/\nu d\nu \quad \text{(ANS absorbance)} \quad (13b)$$

Thus, the difference between the energies of the *trp*-82 excited state and that of bound ANS (weighted for each naphthalene transition L_a and L_b) is 1680 cm^{-1}, and for *trp*-6 is 2137 cm^{-1}. Since the 'bound' spectra are probably influenced by the interaction, we can also calculate these energies from the solution spectra of ANS, and obtain instead 1518 and 1975 cm^{-1}, respectively.

The value of θ for *trp*-82 and ANS is then given by the formula as 19° (31°). The higher value is from assuming the ANS solution value. The interaction energy for *trp*-82 is from 790 cm^{-1} to 550 cm^{-1}.

However, to return to Eqs. (10) (11a) (11b) (12a) (12b) one may note that the expected decay times themselves ought to be recovered from the formalism. Consider that the effective decay constants for the 'new' state are given by

$$\Gamma_{a',b\text{new}} = -(1/\rho_{a'b,\text{new}}) d\rho_{a'b,\text{new}}/dt \quad (14a)$$

while

$$\rho_{a'b,\text{new}} = c_+^2[\cos^2\theta e^{-\gamma_a' t} + \sin^2\theta e^{-\gamma_b' t}] \quad (14b)$$

if one inserts the values for the $\rho_{,\text{old}}(t)$'s from the formulas given in Eqs. (11a) and (11b). If one uses this formula for the decay rates of the 'mixed' states, one can numerically generate two exponential decays with decay-times very similar to those one has input. Alternatively, if instead we rewrote these decays in terms of the original states, we recover the original decay rates for either state identically. In terms of the major decay components this is what we observe for ANS excited at 300 nm in W6Y and nearly so also for *trp* [22]. The major changes between the W6Y decay with and without ANS, or between ANS (in W6YW82Y) *vs* W6Y is in the fraction of decay into the various decay times, not in the values of the times themselves. It is tempting to think that, for W6Y, the 62% fraction decay at $\sim$ 5 ns is the same decay process that is 46% in the presence of ANS (Table 3), or in other words, that 'c_+' in the Eqs. (12a) or (14a) is .46/.62 or .74, the fraction of excited state 'landing' on the excited *trp* surface (relative to that fraction without ANS). If γ_a is taken to be 1/(5.8 ns) and γ_b to be 1/(18.6 ns), then formula (12a) gives the transfer efficiency as 67% for $\theta = 31°$ and 59% for $\theta = 19°$. If, moreover we apply the same correction for fraction of *trp* with ANS bound that we apply in the Table, namely that for W6Y, 15% of the *trp* 18 ns lifetime component is from 'free *trp*' and 85% is from 'bound'(that is, with ANS bound), then one has a corrected 'c_+^2' value of 0.7, which leads to a steady-state quenching as per the formula (13a) of 0.7±.07 (from 31° to 19° respectively) that compares well to the 'observed' extrapolated value of η we found of $\sim$ 0.72.

For W82Y one finds a shift of about 490 cm^{-1} to the red for the bound ANS (data not shown). But this does not admit a solution for θ from our previous formula: $\omega = \sec 2\theta[E_{a'b} - E_{ab'}]$. To that extent there is a failure in our model (or else we must employ imaginary values for θ). The value of c_+^2, corrected for the fraction with bound ANS as before, is 0.92. If one assumes that θ is in fact zero, one obtains an expectation value of steady-state quenching of 0.4, which is fairly comparable to the 0.45 which was the extrapolated 'Scatchard' value. Thus by recourse to data from the bound spectra and from lifetime analysis, we have roughly predicted the values of quenching efficiency that are extrapolated from titrations. It is also of some interest that the c_+^2 values (which indicate how the emissive state is prepared) are close to the values of $\cos^2\theta$, as if the initial probability of the 'old' component in the electronically mixed state is in fact that probability observed at the time of emission, or in other words, the states are only correlated at the instant of excitation, and they then immediately decouple (while if, for W82Y, we now take c_+^2, 0.92, to actually equal $\cos^2\theta$, the value derived for steady-state quenching therein becomes 0.55).

As we see, the degree of dynamical quenching does not comport with the predicted degree of dipole–dipole energy transfer quenching we would calculate, while the coarse outline of a 'mixed' state exciton formalism does at least predict a limiting value of the quenching, as is observed. The degree of dynamical quenching that we do observe can possibly be due to the same adventitious binding (nonspecific binding) we observed in the CD titrations (see Ref. [22]), since we employ rather large concentrations of ANS relative to protein in those studies.

A generalization of the simple variational treatment which we used above is employed in the next investigation (II) to treat the problem of more extensive mixing between two transitions in a single molecule (ANS itself); that treatment also includes the effect of nonzero spatial overlap of the transition densities. The exciton formalism, allowing an equivalence relationship to

be drawn between a spectrum and a (compound) quantum state, is more fully exploited there as well.

We have presented here analyses with mutant versions of rat I-FABP which isolate the effects of single-*trp* residues on the interaction with the unnatural ligand ANS. We have determined the overall similarity of the mutants to the *wt* protein, establishing thereby the relevance of the NMR solution structural studies, performed on the *wt* protein, to understanding the interaction of each single-*trp* with ANS. We have also observed that measures of protein function, such as ligand binding, can be affected by the concentration regime of protein and ligand utilized, which is probably due to the amphipathic (and detergent-like) nature of ANS.

Despite having access to all the necessary input information (distances and angles) to quantitatively predict the 'very-weak coupling' dipole–dipole energy transfer rates, we find the observed energy transfer of *trp*-to-ANS in neither case conforms to very-weak-coupling predictions. We then alternatively invoked a simple model of exciton coupling, which, though not completely satisfactory in some respects, does at least give immediately a maximal energy transfer efficiency very much smaller than the >95% one expects from the Foerster–Dexter mechanism, in more accord with the actual experimental results, and nearly accounts for the observed amount of steady-state quenching in the two proteins.

Acknowledgement

This work was supported by NIH grant GM34847 to F.G.P., in whose laboratory much of this work was performed. The NMR investigations were conducted (as part of Dr. Kurian's thesis) under overall supervision of Nenad Juranic at the Mayo Foundation NMR Core Facility.

Appendix A. Supplementary data

Supplementary data associated with this article can be found, in the online version, at doi:10.1016/j.bpc.2006.07.016.

References

[1] W. Kirk, E. Kurian, F. Prendergast, Characterization of the sources of protein–ligand affinity: 1-sulfonato-8-anilinonaphthalene binding to intestinal fatty acid binding protein, Biophys. J. 70 (1996) 69–83.
[2] I.J. Ropson, C. Frieden, Dynamic NMR spectral analysis and protein folding: identification of a highly populated folding intermediate of rat intestinal fatty acid-binding protein by ^{19}F NMR, Proc. Natl. Acad. Sci. U. S. A. 89 (1992) 7222–7226.
[3] V. Likic, Structure and Dynamics of Internal Water In Rat Intestinal Fatty Acid Binding Protein Thesis, Mayo Graduate School of Medicine, Rochester, Minn, 1999.
[4] S. Wiesner, E. Kurian, F. Prendergast, B. Halle, Water molecules in the binding cavity of intestinal fatty acid binding protein: Dynamic characterization by ^{17}O and ^{2}H magnetic relaxation dispersion, J. Mol. Biol. 286 (1) (1999) 233–246.
[5] V. Likic, F. Prendergast, Structure and dynamics of the fatty acid binding cavity in apo rat intestinal fatty acid binding cavity, Protein Sci. 8 (1999) 1649–1657.
[6] E. Kurian, Solution Structure of Intestinal Fatty Acid Binding Protein complexed with 1-Anilinonaphthalene-8-sulfonate: Implications for Ligand Binding, Thesis, Mayo Graduate School of Medicine, Rochester Minn, 1998.
[7] L. Jaenicke, A rapid micromethod for the determination of nitrogen and phosphate in biological material, Anal. Biochem. 61 (1974) 623–627.
[8] E. Kurian, W. Kirk, F. Prendergast, Affinity of fatty acid for rRat intestinal fatty acid binding protein: further examination, Biochemistry 35 (1996) 3865–3874.
[9] W.R. Kirk, The binding of 1,8 ANS congeners to I-FABP and comparison of some hypotheses about ANS' spectral sensitivity to environment, Biochim. Biophys. Acta 1748 (2005) 84–93.
[10] D.V. O'Connor, D. Phillips, Time-correlated Single Photon Counting, Acad. Press, New York, 1984.
[11] J.M. Beechem, E. Gratton, Fluorescence spectroscopy data analysis environment: a second generation global analysis program, Proc. SPIE 909 (1988) 70–81.
[12] S.Y. Venyaminov, F. Prendergast, Water (H_2O and D_2O) Molar Absorptivity in the 1000–4000 cm^{-1} range and quantitative infrared spectroscopy of aqueous solutions, Anal. Biochem. 248 (1997) 234–245.
[13] N.N. Kalnin, I.A. Baikalov, S. Venyaminov, Quantitative IR spectrophotometry of peptide compounds in water (H_2O) solution. III. Estimation of the protein secondary structure, Biopolymers 30 (1990) 1273–1280.
[14] G. Scapin, J.I. Gordon, J.C. Sacchettini, Refinement of the structure of recombinant rat intestinal fatty acid-binding apoprotein at 1.2-Å resolution, J. Biol. Chem. 267 (1992) 4253–4269.
[15] W. Kabsch, C. Sander, Dictionary of protein secondary structure: pattern recognition of hydrogen-bonded and geometrical features, Biopolymers 22 (1983) 2477–2637.
[16] D. Matulis, R. Lovrien, 1-anilino-8-napthalene sulfonate anion-protein binding depends primarily on ion-pair formation, Biophys. J. 74 (1998) 422–429.
[17] D. Matulis, C. Baumann, V. Bloomfield, R. Lovrien, 1-anilino-8-naphthalene sulfonate as a protein conformational tightening agent, Bioplymers 49 (1999) 451–458.
[18] J. Ory, L. Banaszak, Studies of the ligand binding reaction of adipocyte lipid binding protein using the fluorescent probe 1-anilinonaphthalene, 8-sulfonate, Biophys. J. 77 (1999) 1107–1116.
[19] G. Berden, L. Meerts, D. Plusquellic, I. Fujita, D. Pratt, High resolution electronic spectroscopy of 1-aminonaphthalene: S_0 and S_1 geometries and $S_1 \leftarrow S_0$ transition moment orientations, J. Chem. Phys. 104 (1996) 3935–3946.
[20] P. Callis, $^{1}L_a$ and $^{1}L_b$ transitions of tryptophan: applications of theory and experimental observations to fluorescence of proteins, Methods Enzymol. 278 (1997) 113–150.
[21] Th. Fœrster, Delocalized excitation and excitation transfer, in: Oktay Sinanoglu (Ed.), Modern Quantum Chemistry, Academic Pr. N.Y, 1964, pp. 93–137.
[22] What is difficult to account for is the effect of long range d–d energy transfer and nonspecific binding of ANS under these conditions — the so-called critical concentration of ANS-*trp* (21) is about 5 mM=3000/$4\pi R_0{}^3 N_0$ significantly greater than the 60 μM we employ, but the possibility looms large that some quenching is contributed by nonspecifically bound ANS in another location on FABP.
[23] S.W. Provencher, J. Glockner, Estimation of globular protein secondary structure from circular dichroism, Biochemistry 20 (1981) 33–37.
[24] P. Manavalan, W. Johnson Jr., Variable selection method improves the prediction of protein secondary structure from circular dichroism, Anal. Biochem. 167 (1987) 76–85.
[25] N. Sreerama, S. Yu.Venyaminov, R.W. Woody, Estimation of the number of α-helical and β-strand segments in proteins using circular dichroism spectroscopy, Protein Sci. 8 (1999) 370–380.
[26] J.P. Hennessey, W.C. Johnson Jr., Information content in the circular dichroism of proteins, Biochemistry 20 (1981) 1085–1094.
[27] S. Yu.Venyaminov, J.T. Yang, in: G.D. Fasman (Ed.), Circular Dichroism and the Conformational Analysis of Biomolecules, Plenum Press, New York, 1996, pp. 69–107.

[28] We give a short description of the singular value decomposition and ridge regression methods: SVD is similar to the principal axis rotation method we employ for the 'exciton formalism' — where, however, the observed output data, a matrix **Y**, say, of the CD obtained with a basis set of proteins (with input structures **X**) at different wavelengths, multiplied by its transpose: or $\mathbf{Y}^t\mathbf{Y}$, now a symmetric matrix, is 'rotated' to diagonal form, thus displaying its eigenvalues, which are assumed to be characteristic for all secondary structural features. Thus $\mathbf{Y}^t\mathbf{Y}=\mathbf{U}\mathbf{S}^2\,\mathbf{U}^t$ with **U** a unitary and $\mathbf{S}^2$ a diagonal matrix, one then finds **V** (also unitary, but $\dim\mathbf{U}\neq\dim\mathbf{V}$) fulfilling $\mathbf{V}=\mathbf{Y}\mathbf{U}\mathbf{S}^{-1}$ such that $\mathbf{Y}=\mathbf{V}\mathbf{S}\mathbf{U}^t$, the **S** terms are the singular values of **Y**. In ridge regression, square regression is minimized (as in *least* squares) subject to a constraint, namely that there be a large positive weight (λ) on data on the diagonal, i.e. that the found predictors be 'near' a set of singular values, hence a 'ridge' of solutions, so that the predictor of CD output given input basis **X**, called **P**, is such that: $\mathbf{P}=\mathbf{X}^t\mathbf{Y}(\mathbf{X}^t\mathbf{X}-\lambda\mathbf{I})^{-1}$.